# A Computational Fluid Dynamics Model of a Spinning Pipe Gas Lens

C. Mafusire*[a,b], A. Forbes[a,b,c], G. Snedden[d]
[a]CSIR National Laser Centre, P. O. Box 395, Pretoria, South Africa
[b]School of Physics, University of KwaZulu–Natal, Private Bag X54001, Durban 4000, South Africa
[c]Stellenbosch University, Private Bag X1, Matieland 7602, South Africa
[d]CSIR Defence Peace Safety Security, P. O. Box 395, Pretoria, South Africa

## ABSTRACT

When a metal horizontal pipe is heated and spun along its axis, a graded refractive index distribution is generated which is can be used as a lens, thus its name, the spinning pipe gas lens (SPGL). Experimental results showed that though increase in rotation speed and/or temperature resulted in a stronger lens and removed distortions due to gravity, it also increased the size of higher order aberrations resulting in an increase in the beam quality factor ($M^2$). A computational fluid dynamics (CFD) model was prepared to simulate the aerodynamics that show how it operates and, in the process shed some light on the optical results. The results of the model consist of velocity profiles and the resultant density data and profiles. At rest the cross-sectional density profile has a vertical symmetry due to gravity but becomes rotationally symmetric with a higher value of density at the core as rotation speed increases. The longitudinal density distribution is shown to be parabolic towards the ends but is fairly uniform at the centre. The velocity profiles show that this centre is the possible source of higher order aberrations which are responsible for the deterioration of beam quality.

**Keywords**. Computational fluid dynamics (CFD), Spinning pipe gas lens (SPGL), Optical aberrations

## 1. INTRODUCTION

If a heated steel pipe made to rotate (spin) about its axis, a graded density profile is formed across the diameter of the pipe which, in turn, results in a graded refractive index profile. Under certain conditions, this profile leads to wave guiding, and with judicious choice of pipe length, a laser beam propagating along its axis converges in space on exit. When this happens, the system is seen to act as a lens, and is referred to as a spinning pipe gas lens (SPGL). The device was invented by Martynenko[1] (1975) and subsequently gained popularity as a device for high power laser delivery. It has been used for focusing high power lasers[2,3] and as a telescope objective[4]. Recently, measurements based on wavefront analysis using the Shack-Hartmann wavefront sensor were performed which showed that increasing the wall temperature and rotation speed result in a deleterious effect on any light beam propagating through it[5-7]. Included were investigations based on a computational fluid dynamics (CFD) of the lens. In this paper we investigate the model a little further discussing the heat and mass transfer properties which make the lens work but at the same time introduces higher order aberrations.

The concept of focusing is associated with the size of a laser beam being progressively reduced until it reaches a minimum. This can be achieved when the beam experiences less phase delay at the edges than along the axis, an effect which has a parabolic relationship with radial distance. The property of a particular medium that causes the beam to change is the refractive index which causes the beam to deflect towards higher refractive index. One way we can achieve this is to put a lens in the path of the beam. It works by delaying the phase of the beam at the edges than along the axis, i.e., the edges are refracted more at the edges than along the axis resulting in one plane in which the beam size is minimum called the focal plane, the distance to which is called the focal length. The spinning pipe gas lens works as a positive lens and in that the density along the axis is higher along the axis than along the walls. This effect can be explained using the Gladstone-Dale law which is given by the equation $n = G\rho + 1$. This equation relates local density, $\rho$, of a fluid to refractive index, $n$ where $G$ is the Gladstone-Dale constant ($2.23 \times 10^{-4}$ m$^3$/kg for air). The performance of the gas lens is a result of the fact that if the walls of the pipe are heated, then rotated along the axis. The movement of the walls causes the heated air to co rotate with the pipe. By Newton's third law of motion, the co rotating air is centrifugally

* cmafusire@csir.co.za; phone +27 12 841 3900; fax +27 12 841 3152

Laser Beam Shaping XI, edited by Andrew Forbes, Todd E. Lizotte, Proc. of SPIE Vol. 7789, 77890Y · © 2010 SPIE · CCC code: 0277-786X/10/$18 · doi: 10.1117/12.862857

expelled and is replaced by cooler air from the surrounding which is sucked along the axis. This means the density has a graded distribution which results on the gas lens being a graded refractive index (GRIN) lens. The power of the lens is increased by increasing the rotation speed and/or wall temperature in that they result in the hot air being expelled faster and the cold air sucked in faster and further before it assumes the temperature of the walls. For focusing to take place, the necessary and sufficient conditions are that the rotation speed must be greater than zero and the wall temperature must above the ambient.

The other aspect that is observed in aerodynamic media is that of random density fluctuations. In the SPGL, this is a result of the interaction of heated air being expelled with cold air from the environment. These density fluctuations result in refractive index fluctuations. We can assume that the refractive index can be represented by $n = n(r, z)$ where $r$ and $z$ are the radial and longitudinal spatial co ordinates respectively. If the geometrical length of the laser beam path in the SPGL is given by, $l$, then the phase change experienced by the beam is given by $\phi(r, z) = kln(r, z)$ where $k$ is the laser beam wave constant. This means that the distortions in the gas lens can be measured by observing the phase changes in the laser beam. Distortions to an optical wave are called optical aberrations[8,9]. The most current method of representation is the use of Zernike coefficients which are based on a polynomial system with which the optical behaviour associated with each aberration can be defined.

The paper is organized as follows. Section 2 discusses the flow in the SPGL in some detail showing the source of the flow which results in the density conducive to focusing. The CFD model and its results are presented in section 3 to help show the source of these aberrations. Results from a previous publication on the experimental investigation on the SPGL are presented in section 4. The paper is concluded in section 5.

## 2. ZERNIKE POLYNMIALS

The phase of a wavefront in a circle can be written as a linear combination of Zernike polynomials. Zernike functions are unique in that they are the only polynomial system in cylindrical co-ordinates which are orthogonal over a unit circle, invariant in form with respect to rotation of the co-ordinate system axis about the origin and include a polynomial for each set of radial and azimuthal orders. The polynomials are a set of orthogonal polynomials that arise in the expansion of a wavefront function for optical systems with circular pupils. The expansion of an arbitrary phase function, $\phi(\rho, \theta)$ where $\rho \in [0,1]$ and $\theta \in [0, 2\pi]$, in an infinite series of these polynomials will be complete. The radial polynomial, $\rho$, is normalised by the Zernike radius and is given by $r/a$. The circle polynomials of Zernike have the form of complex angular function modulated by a real radial polynomial. Using the Born and Wolf notation[8], we can represent each Zernike term by:

$$Z_{nm}(\rho, \theta) = R_{nm}(\rho)\Theta_m(\theta) \tag{1}$$

The angular part is defined as:

$$\Theta_m(\theta) = \begin{cases} \cos(m\theta), & m > 0 \\ \sin(m\theta), & m < 0 \\ 1, & m = 0 \end{cases} \tag{2}$$

whereas the radial part is a polynomial given by:

$$R_{nm}(\rho) = \sum_{k=0}^{\frac{n-m}{2}} \frac{(-1)^k (n-k)! \rho^{n-2k}}{k!\left(\frac{n+m}{2}-k\right)!\left(\frac{n-m}{2}-k\right)!} \tag{3}$$

where $n$ and $m$ are the order and the ordinal numbers respectively. The order is a non-negative integer which is related to $m$ such that $|m| \le n$ and $n - m$ is even. This means that for every $n$, $m$ goes from $-n$ to $n$ in steps of 2. A few of the

radial terms, up to the fourth order, are listed in the Table 1. Contour plots of these Zernike polynomials are shown in Table 2.

Table 1 Radial Zernike polynomials up to the fourth order

| *n* | *m* | | | | |
|---|---|---|---|---|---|
| | 0 | 1 | 2 | 3 | 4 |
| 0 | $1$ | | | | |
| 1 | | $\rho$ | | | |
| 2 | $2\rho^2-1$ | | $\rho^2$ | | |
| 3 | | $3\rho^3-2\rho$ | | $\rho^3$ | |
| 4 | $6\rho^2-6\rho^2+1$ | | $4\rho^4-3\rho^2$ | | $\rho^4$ |

Table 2 Contour plots of the Zernike primary aberration polynomials

| *n* | *m* | | | | | | |
|---|---|---|---|---|---|---|---|
| | -3 | -2 | -1 | 0 | 1 | 2 | 3 |
| 0 | | | | | | | |
| 1 | | | | | | | |
| 2 | | | | | | | |
| 3 | | | | | | | |
| 4 | | | | | | | |

This means that a laser beam wavefront described by a phase function $\phi(\rho,\theta)$ can be expanded as a linear combination of an infinite number of Zernike polynomials, using generalized coefficients as follows:

$$\phi(\rho,\theta)=\sum_{n=0}^{\infty}A_{n0}R_{n0}+\sum_{n=1}^{\infty}\sum_{m=1}^{n}R_{nm}\left[A_{nm}\cos(m\theta)+B_{nm}\sin(m\theta)\right] \tag{4}$$

The *A* and *B* terms are referred to as the symmetric and non-symmetric terms, respectively. The process of finding this equation involves the extracting the Zernike coefficients $A_{nm}$ and $B_{nm}$, each one corresponding to a particular aberration, by a process of fitting Eq. (4) to a given wavefront. Since the Zernike set is an infinite set, it is always practical to select a finite maximum order, *n*, to express a particular wavefront. This is practical in that in optical systems, the coefficients get smaller and smaller as the order increases. The value of zero, or at least a very small value, for a particular aberration coefficient signifies its nonexistence or that it is insignificant that it can be ignored. If the phase is known as a function, then the *rms* Zernike coefficients $A_{nm}$ and $B_{nm}$ can are calculated using the Eq. (5).

$$A_{nm}=\frac{1}{\pi}\sqrt{\frac{2(n+1)}{1+\delta_{m0}}}\int_0^{2\pi}\int_0^1\phi(\rho,\theta)R_{nm}\cos(m\theta)\rho d\rho d\theta \tag{5a}$$

$$B_{nm} = \frac{1}{\pi}\sqrt{\frac{2(n+1)}{1+\delta_{m0}}}\int_0^{2\pi}\int_0^1 \phi(\rho,\theta)R_{nm}\sin(m\theta)\rho d\rho d\theta \qquad (5b)$$

where $\delta$ is the Kronecker delta function and the integrals' coefficients are normalizing constants. Note that $B_{nm} = 0$, whenever $m = 0$, a fact which can be confirmed by Eq. (5b). The names of the coefficients whose plots are shown in Table 2 are given in Table 3. There are classified as primary, secondary, tertiary and so on. Primary aberrations are of the lowest with the order increasing for secondary and then tertiary up to infinity. Experience and research has shown the impact of the aberrations decreases with increasing order and so for most practical purposes depending on the experiment, the maximum order can be specified with all terms above it ignored. In this paper we are going to concentrate on primary aberrations called tilt, defocus, spherical aberration, astigmatism and coma. In terms of density distribution in an SPGL, tilt is associated with linear density gradient associated with, say, gravity in a non-rotating SPGL whereas defocus is associated with parabolic density distribution in a rotating SPGL. Spherical aberration is associated with a quartic density distribution and as will be explained later, is associated with gas exchanges in the boundary layer. Astigmatism and coma and are more complicated and are not immediately associated with a particular aspect of the flow in the SPGL.

Table 3 The names of the Zernike primary aberration coefficients

| *n* | *m* | **Description and symbol** |
|---|---|---|
| 0 | 0 | Piston, $A_{00}$ |
| 1 | -1 | *x*-Tilt, $B_{11}$ |
| 1 | 1 | *y*-Tilt, $A_{11}$ |
| 2 | -2 | *y*-Primary Astigmatism, $B_{22}$ |
| 2 | 0 | Defocus, $A_{20}$ |
| 2 | 2 | *x*-Primary Astigmatism, $A_{22}$ |
| 3 | -3 | *y*-Triangular Astigmatism, $B_{33}$ |
| 3 | -1 | *y*-Primary Coma, $B_{31}$ |
| 3 | 1 | *x*-Primary Coma, $A_{31}$ |
| 3 | 3 | *x*-Triangular Astigmatism, $A_{33}$ |
| 4 | 0 | Spherical Aberration, $A_{40}$ |

## 3. NUMERICAL RESULTS

To confirm the theoretical analysis of an SPGL given above and the optical aberrations measured from its performance[5-7], a computational fluid dynamics (CFD) simulation of a simplified test system was executed using the commercial CFD code, STAR–CD® using the $k-\varepsilon$ model[10,11]. The purpose of this study is to show the effect of the heat and mass transfer on the velocity distribution and density. Assumptions included the removal of the mounts and other three-dimensional geometry features that would complicate the geometric model. The pipe used in the model is based on the dimensions of the actual SPGL we have in the laboratory. It is 1.43 m long and an internal diameter of 0.0366 m. The heated section is about 0.91 m long which means the heated ends are about 0.25 m each. The pipe is accurately reproduced with the further assumption that the mounts act as a heat sink and thus the pipe ends are unheated. A fully transient solution is presented in which the pipe is spun up from a heated (a temperature of 100 ºC) steady-state buoyancy-driven solution, and held at fixed speed of 20 Hz until a steady state has been reached.

The mesh used in the solution consisted of 350 transverse slices regularly arranged along the pipe's length. Each slice consisted of 512 nodes distributed across the section with more nodes concentrated along the boundary (see Figure 1). The results extracted from the model included density for each data point in the centre of the cell in the mesh and

animations showing the evolution of the velocity and density at selected transverse and longitudinal cross-sections. Temperature distribution was extracted from the density data.

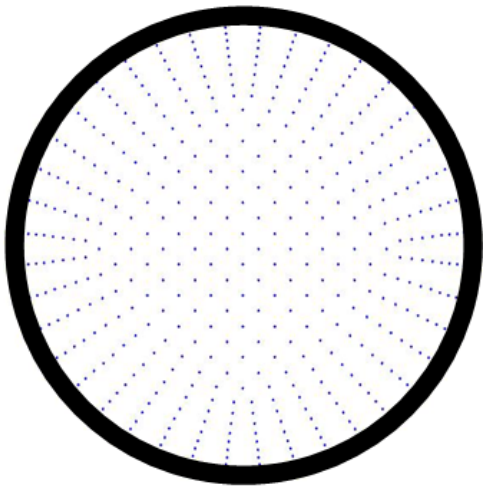

Figure 1. The SPGL mesh transverse cross-section used in the CFD model.

### 3.1 Velocity profiled

Figure 2 (a) is a longitudinal cross-section of the gas lens showing velocity distribution for the left end on top, the mid-section at the centre and the bottom part at the bottom with a key showing the speed. The velocity distribution at the ends in the unheated section is dominated by transverse movement of air towards the centre from both sides in the inviscid section outwards along the boundary section with rotation playing very little or no part. As one gets further inside, the transverse speed of incoming air decays as it gets further inside, the length of which increases with increase in wall temperature and/or rotation speed. Inversely, as one gets further inside, the effect of the rotation increases as the transverse speed decreases and you have pure rotation right at the centre. In the boundary layer, the expelled air is fastest as it exits from the pipe. Before exit, the boundary is a combination of translation and rotation, which means this layer, expels hot air in a spiral motion in opposite directions away from the centre. From this velocity distribution, we can have a feel of the heat distribution in the inviscid region since fast moving air accumulates transversely injected heat much more slowly compared to stationary air. This means the incoming air is cooler but accumulates heat as it slows down and approaches the centre. This might point to a situation where the temperature along the axis at the centre is higher than that of the walls since because of the particles' slow velocity, they accumulate heat over time.

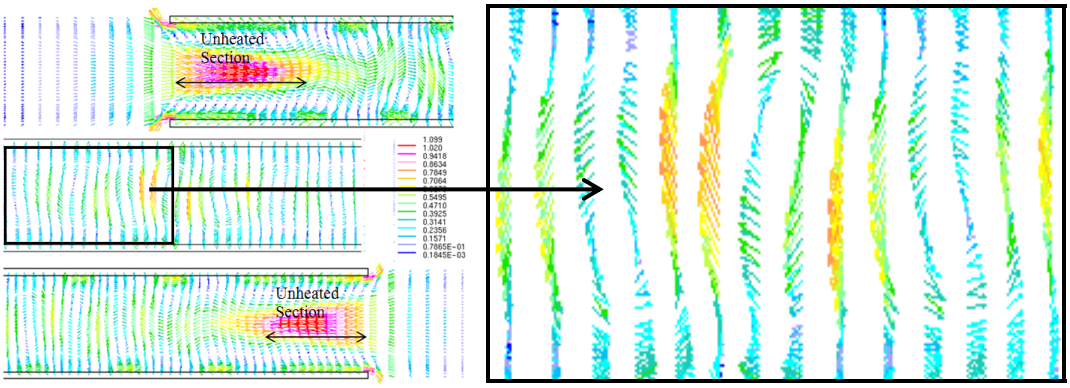


(a) (b)

Figure 2. Velocity profiles in the SPGL for the end sections (above and below), the mid-section in the middle (a). A closer profile shows the cyclic nature of the localised velocity distributions (b).

A closer look at the velocity profile Figure 2 (b) shows the complicated velocity distribution away from ends of the pipe. Besides the transverse flow, the velocity distribution shows that there is less longitudinal flow but more localised

oscillations as one shows that from plane to plane that this is not regular. This could be evidence of multi-cellular flow. It is this irregularity which is most likely responsible for the presence of coma, astigmatism and other higher order aberrations. This oscillatory activity is expected to increase with increase in wall temperature or rotation speed which in turn, increases the size of these aberrations.

### 3.2 Density

The initial state in a heated stationary heated SPGL is a result of natural convection. This is shown in Figure 3 (a) which is a CFD created density distribution near the end face of the pipe. It shows the density gradient which is proportional to height. At rotation speed of 20 Hz, the density gradient has disappeared and the density has rotational symmetry due to forced convection with the highest density along the axis, a density distribution conducive to focusing (Figure 3 (b)). Note that the density at the edges of the profile is lower than the density immediately inside, a result that will be discussed later. The aberration measurements show the tilt is the dominant aberration in the stationary case but it is reduced to a very low value during rotation with defocus becomes dominant.

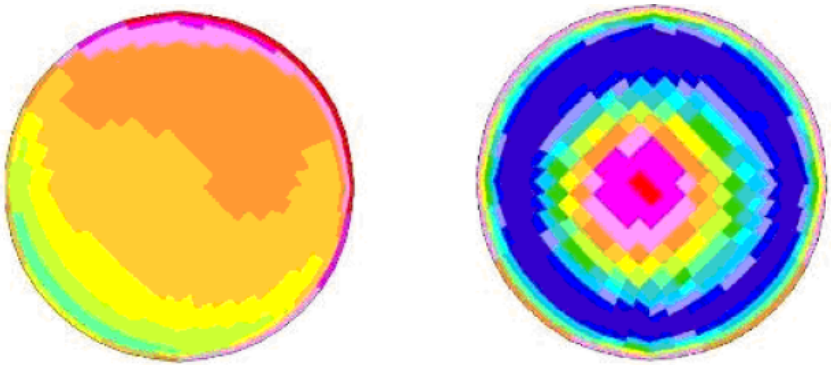

(a) (b)

Figure 3. Cross–sectional density profiles of an SPGL showing: (a) the initial state after heating, and (b) the rotating steady–state near the end face of the pipe, with high density centre (red) and low density edges (blue).

The other results from the density calculations confirm the velocity profile from the previous sub-section. Temperature ($T$) distribution was extracted from the density ($\rho$) data using the equation, $\rho = \rho_o\left(1-\alpha(T-T_o)\right)$ where $\alpha$ = $2.263123\times10^{-4}$ $K^{-1}$ is the coefficient of volume expansion of air and $\rho_o$ is the known density at a known temperature, $T_o$ say at room temperature. Figure 4 (a) shows a plot of the density profile of the longitudinal section pipe which includes the axis. It also shows density distributions in transverse sections at critical planes. The respective temperature profile, (Figure 4 (b)) show that the unheated section is at room temperature (27 ºC) and the centre of the pipe is at about 100 ºC, the temperature of the wall.

Looking at these two profiles we can also see the effect of the cold air entering form both ends which slows down and heats up at the same time. This results in the parabolic profile which is responsible for the lensing effect. As can be observed in the transverse profiles, a parabolic density distribution is only evident in a short section of the entire length, possibly less than half. This length should increases with both rotation speed and temperature making the lens stronger. Closer look at the cross-section profiles in Figure 4 (a) shows that some of them have a quartic density distribution though for a very shorter length compared to the purely parabolic profile the size of which should also increase with rotation speed or temperature. This is the source of the spherical aberration which has been shown to increase with rotation speed and/or temperature.

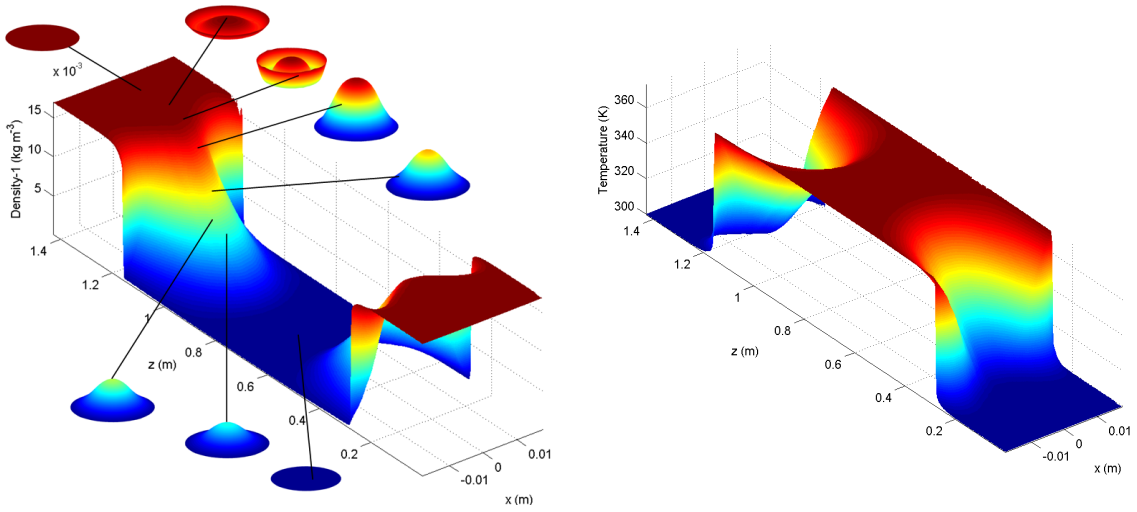


(a) (b)

Figure 4. A 3D longitudinal density profile for the SPGL showing transverse sections at critical planes with 2D profile (b) shows the plot for further elucidation (a). The transverse density profile at the centre of the SPGL (c)

Another interesting result is the transverse temperature profile of the centre, i.e. away from the face ends, which shows that the temperature along the axis is just over 0.16 K higher than at the walls (Figure 5 (a)) corresponding to a density 4 $\times$ $10^{-5}$ kg $m^{-3}$ lower than at the walls (Figure 5 (b)). The explanation for this is that because air particles at this part of the pipe are moving very slowly and thus accumulates heat faster due to both convection and conduction as discussed in the subsection above resulting in an opposite relationship in density. Combining this information and the velocity distribution discussed in the previous sub-section, we have a fairly good idea what causes coma and astigmatism and other higher order aberrations.

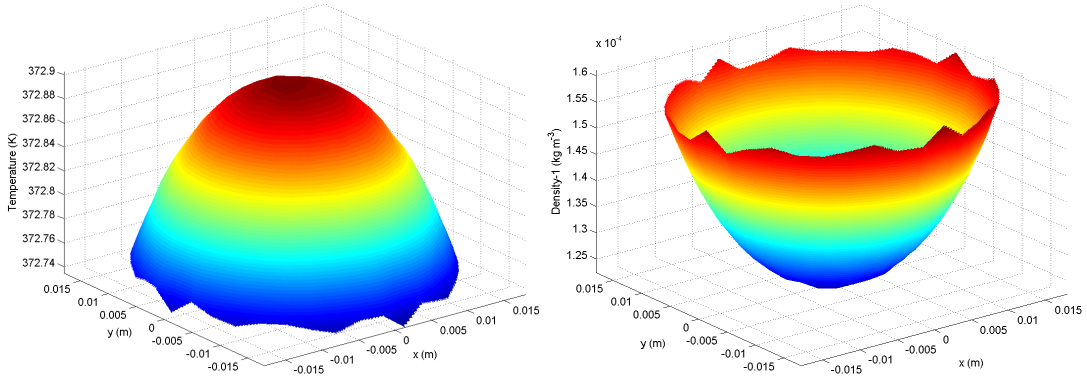


(a) (b)

Figure 5. The transverse temperature (a) and density (b) profiles at the centre of the SPGL

## 4. EXPRIMENTAL INVESTIGATION

Since density is directly proportional to refractive index, the phase of a laser beam propagating through a spinning pipe gas will be altered depending on the refractive index distribution in an SPGL. Foe completeness, we present a summary of the optical investigation on the aberrations generated by an actual SPGL that was carried with a Shack-Hartmann wavefront sensor[5]. An expanded HeNe laser beam steered by flat mirrors is made to propagate through the lens. A Shack-Hartmann wavefront sensor was placed just behind the lens and used to measure the beam's quality and phase aberrations for rotation speeds up to about 17 Hz for wall temperatures 351, 373, 400 and 422 K.

The first result confirms the fact that rotation removes distortions which are caused by gravity by the way in which by the way in which *y*-tilt which is induced by gravity is reduced to a bare minimum as soon as rotation commences (Figure 6 (a)) whereas *x*-tilt remains a very small (Figure 6 (b)). We can observe the same effect by looking the phase distribution before and during rotation. Figures 7 (a) and (b) show the phase distribution before and during rotation, respectively. The phase maps are dominated by *y*-tilt and defocus, respectively. However, digital removal of defocus and tilt reveals the presence of higher order aberrations. The resulting phase map is shown in Figure 7 (c). This phase map helps illustrate the other result observed during the experiment, the effect of the SPGL on the beam quality factor.

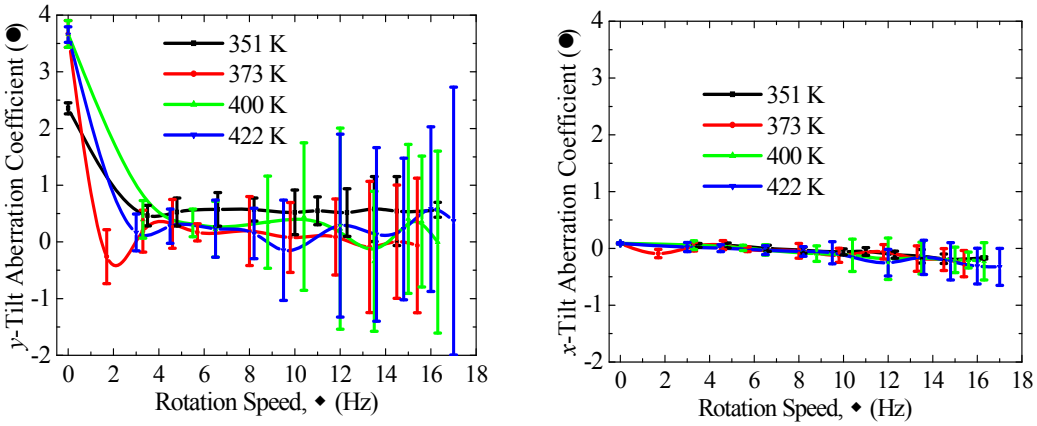


(a) (b)

Figure 6. (a) *y*–tilt and (b) *x*–tilt generated by a spinning pipe gas lens at selected wall temperatures and rotation speeds.

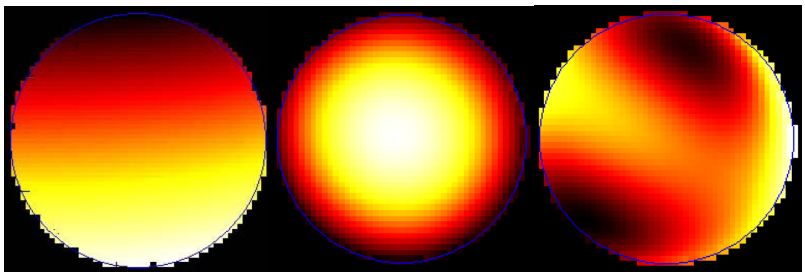

(a) (b) (c)

Figure 7. The phase distribution of the laser beam with: (a) no rotation but heated to 422 K, showing tilt; (b) after rotating the SPGL at 17 Hz, showing significant curvature on the wavefront; and (c) same conditions as in (b) but with defocus and tilt removed, revealing the higher order aberrations.

Study of other aberrations shows that they increase in size as rotation speeds and/or wall temperature is increased (Figure 8 (a)) thereby increasing the beam quality factor, $M^2$ (Figure 8 (b)). This confirms the fact that the SPGL also generates aberrations which are increasing in power as the lens becomes stronger.

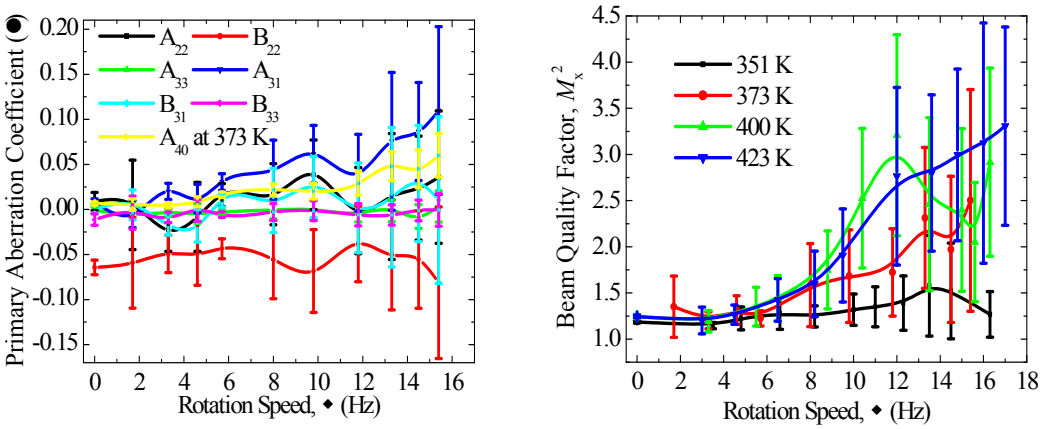


(a) (b)

Figure 8. (a) Higher order aberrations introduced by the SPGL; (b) increase in $M_x^2$ with rotation speed and temperature as a direct result of the aberrations in (a).

## 5. CONCLUSION

We have used a computational fluid dynamics model of the spinning pipe gas lens to show how the lens operates, in the process generate aberrations which, incidentally increase when both rotation speed and temperature are increased. The CFD model has shown that the density gradient is linear before rotation but becomes rotationally symmetric with the highest density along the axis. In sections of the SPGL, the cross-section density has a quartic distribution. The centre, however, is dominated by high temperatures with irregularly distributed velocity distribution and is the most likely source of other optical aberrations such as coma and astigmatism.

## REFERENCES


[1] Martynenko, O. G., "Aerothemooptics" International J. of Heat and Mass Transfer. 18, 793–796 (1975).

[2] Michaelis M. M., Notcutt M., and Cunningham P. F., "Drilling by a Gas Lens Focused Laser", Opt. Comm. 59, 369–374 (1986).

[3] Michaelis M. M., Kuppen M., Forbes A., Viranna N., and Lisi N., "Progress with gas lenses", Laser and Particle Beams 14, 473–485 (1996).

[4] Michaelis M. M., Dempers C. A., Kosch A. M., Prause A., Notcutt M., Cunningham P. F, and Waltham J., "Gas lens telescopy", Nature 353, 547-548 (1991).

[5] Mafusire, C., Forbes, A., Michaelis, M. M., and Snedden, G "Characterization of a spinning pipe gas lens using a Shack-Hartmann wavefront sensor", Laser Beam Shaping VIII, Ed. F. Dickey, Proc. SPIE., **6663** 6663H (2007).

[6] Mafusire, C., Forbes, A., Michaelis, M. M., and Snedden, G "Optical aberrations in a spinning pipe gas lens", Opt. Exp., 16 (13) 9850-9856 (2008).

[7] Mafusire, C., Forbes, A., Michaelis, M. M., and Snedden, G "Spinning pipe gas lens revisited", SA. J. Sc., 104.

[8] Born, M. and Wolf, E. 1999 [Principles of Optics: Electromagnetic theory of propagation, interference and diffraction of light 7th Ed] Cambridge University Press, Cambridge 517-553 (1998).

[9] Mahajan, V. N., [Optical Imaging and Aberrations, Part I: Ray Geometrical Optics] SPIE Press (1998).

[10] Davison, L., "An Introduction to Turbulence Models. Chalmers University of Technology", Downloaded online on 19-07-2010 from: www.tfd.chalmers.se/~lada/postscript_files/kompendium_turb.pdf

[11] Blazek, J. [Computational Fluid Dynamics - Principles and Applications] Ch 7 Elvesier, Oxford (2001).